An Experimental and Computational Study of Flowfields in a Louvered Fin Heat Exchanger

L. Winston Zhang[1], Steve B. Memory and Jonathan P. Wattelet
Modine Manufacturing Company
1500 DeKoven Avenue
Racine, WI 53403-2552

Marlow E. Springer and Karen A. Thole
Mechanical Engineering Department
University of Wisconsin
Madison, WI 53706-1572

ABSTRACT

This paper presents an experimental and computational study of flowfields in a louvered fin heat exchanger. The experimental work on flowfield characteristics is conducted using the laser doppler velocimetry (LDV) technique on a 20:1 scaled-up model of a 19-row louvered fin array with a louver angle (θ) of 27° and a louver-to-fin pitch ratio (F_p/L_p) of 0.76. These measurements are performed at two different Reynolds numbers, Re_{Lp} = 230 and 1016, based on louver pitch and inlet face velocity. Computational fluid dynamics (CFD) predictions are performed for flow over one periodic louver array, assuming two-dimensional laminar flow.

In general, good agreement for both bulk flow and boundary layer flow characteristics is found between the experimental measurements and computational predictions for all conditions. Bulk flow characteristics also show the development of the flow from louver to louver and the impact of wakes from upstream louvers on downstream louvers. It is clearly seen that the flow has become louver directed by the second louver. Boundary layer measurements of velocity profiles also help to shed light on local heat transfer behavior in louvered fin surfaces. CFD predictions further highlight different flow regimes within the Reynolds number range of 50~2,000. These heat transfer results not only confirm the flow characteristics discovered from the corresponding flowfield study but also identify the operating heat transfer enhancement mechanisms of louvered fin heat exchangers.

INTRODUCTION

Louvered fin heat exchangers have been used extensively in automotive applications such as radiators, oil coolers, condensers and charge air coolers. The dominant thermal resistance in these types of heat exchangers is typically on the air-side where the flow characteristics can be quite complex. Louvers form continuous interruptions, which break up the growth of the laminar boundary layer that naturally, forms along each louver, thereby forming new boundary layers on downstream louvers with associated higher heat transfer.

Louvered fin studies date back to the flow visualization work performed by Beauvais (1965) using smoke traces. Based on his observations, Beauvais argued that the heat transfer in the first section of each louver could be treated as laminar flow over a flat plate, whereas further downstream, it can be approximated by laminar flow in a duct with a parabolic velocity

[1] Author to whom correspondence should be addressed.

distribution. Davenport (1983) performed flow visualization experiments identical to those of Beauavis and found the flow characteristics to be a function of Reynolds number. He also discovered that the friction factor was close to that given by the Blasius solution for a flat plate at low Reynolds numbers but flattened at higher Reynolds numbers, where characteristics of both friction and form drag were evident. The heat transfer and pressure drop studies by Achaichia and Cowell (1988a) also identified two flow conditions, a "duct" and "louver" directed flow at low and high Reynolds numbers, respectively. However, in contradiction to Davenport, they found that at high Reynolds numbers the Stanton number curve ran parallel to, but lower than that of laminar boundary layer flow over a flat plate, while at low Reynolds numbers, it showed similar characteristics to that of laminar duct flow.

Webb and Trauger (1991) performed flow visualization in louvered fins using a dye injection technique for a Reynolds number range of 400 to 4,000. They defined a dimensionless quantity called "flow efficiency" given as the ratio of *mean* flow angle to louver angle. For a given set of geometrical parameters, the flow efficiency increased with the Reynolds number. The only detailed flowfield measurements given in the open literature were performed by Antoniou et al. (1990) who used a hot-wire anemometer in a 16:1 scaled-up louver array model. They presented flowfield results for three different Reynolds numbers ranging from 500 to 2,300 ($\theta = 25°$, $F_P/L_P = 1.7$). Their results indicated an increase in the mean flow angle for each stream-wise louver until approximately the fourth louver position. Beyond the fourth louver, the mean flow angle approached 92% of the louver angle over the range of Reynolds numbers investigated. Downstream of the middle-turning louver, the flow took longer to re-adjust, particularly at lower Reynolds numbers. One problem with hot-wire anemometry, of course, is its intrusive nature.

With regard to computational work, Achaichia and Cowell (1988b) simulated flow through a louvered fin array by modeling two-dimensional, fully developed and steady laminar flow over a large number of single louvers ($\theta = 15\text{-}55°$, $F_P/L_P = 1.0\text{-}2.5$), with periodic boundary conditions in both directions. Their analysis showed that as the Reynolds number increased, the mean flow angle approached the louver angle to within a few degrees, confirming their earlier experimental work which identified a transition from "duct" to "louver" directed flow. Using intuitive geometric analysis, Suga and Aoki (1991) proposed a simple expression to represent the optimum geometric relation between θ and F_P/L_P by controlling the distribution of the thermal wake produced from an upstream louver:

$$F_P/L_P = 1.5 \tan\theta \qquad (1)$$

This equation was "verified" numerically using a two-dimensional finite difference code. They found that their results were independent of Reynolds number for the range they considered ($64 < Re_{L_P} < 450$). The louver array geometry ($F_P/L_P = 0.76$) adopted in the present study was "predicted" using equation (1) based on a louver angle of 27°. Zhang (1996) simulated both steady and unsteady two-dimensional flows over a single louver using the same periodic domain ($\theta = 25°$, $F_P/L_P = 1.25$) and found similar results. In addition, at high Reynolds numbers ($Re_{L_P} > 782$), he also predicted vortex shedding from both the front and back leading edges of the louver.

This paper presents a two-pronged approach that compares non-intrusive laser doppler velocimetry (LDV) measurements of flowfields in a 20:1 scaled-up louver array with those predicted numerically using computational fluid dynamics (CFD). Both methods are based on two-dimensional models, thereby neglecting the effect of the tubes. Comparison is limited to two Reynolds numbers, 230 and 1016, both in the steady laminar flow regime. Measurements include both bulk flow and boundary layer characteristics in an attempt to clarify some of the

discrepancies mentioned above. Finally, the paper provides some insight into how heat transfer is affected by these flow characteristics and highlights the important enhancement mechanisms of louvered fin heat exchangers.

EXPERIMENTAL AND NUMERICAL APPROACHES

The studies discussed in this section deal with a louvered fin-and-tube design as illustrated in Figure 1a. The main focus is on the louvered fin array with the geometrical parameters of interest illustrated in Figure 1b and Figure 1c. Table 1 summarizes the louvered fin geometry.

Table 1. Summary of Louvered Fin Geometry

Louver Angle (θ)	27°
Fin Pitch to Louver Pitch Ratio (F_P / L_P)	0.76
Fin Thickness to Louver Pitch Ratio (t / L_P)	0.08
Number of Louvers per Louver Array	17
Vertical Louver Distance to Louver Pitch (H_l/ L_P)	0.67

For the experiments, a 20:1 scaled-up model was placed in the test apparatus shown in Figure 2a. A settling chamber was placed upstream of the test section to condition the flow entering the test section. At the entrance to the test section, screens and popcorn foam were used to straighten the incoming flow and achieve flow uniformity with reduced turbulence intensity. A 12 W (1/64 HP) in-line axial fan running at 3500 rpm propelled the flow. A manual butterfly valve was used to control the flow rates to achieve the required inlet flow Reynolds numbers. The inlet face velocity was 0.141 m/s and 0.582 m/s for Re_{Lp} = 230 and 1016 respectively. Due to the blockage caused by the fin thickness, actual velocities entering the louver passage were 12% higher.

To provide enough louver rows to ensure periodic flow in a number of the passages, the test section was designed using CFD (Springer and Thole, 1998). Nineteen louver rows were found to be sufficient in that they provided approximately four louver passages (shown shaded in Figure 2a) through which the flow was predicted to be periodic. This was experimentally verified by Springer and Thole (1998). In addition, the location of the top wall was placed $3F_P$ away from the nearest row of louvers and the bottom wall was placed $0.5F_P$ from the bottom row of louvers. A larger spacing was needed on the top wall to allow the flow to turn and enter the louvers downstream of the turning louver. To provide optical access, 12.5 mm Lexan front and back plates were used. The fins themselves were made from 2.28 mm thick cold rolled steel, anodized to reduce laser beam reflections. Magnification of the louver indicated a slight radius to the edges of each louver. The dimensions of the scaled-up test section were 17.5 cm deep, 44.1 cm high and 69.6 cm long.

To avoid the boundary layer that forms on the side-walls of the test section, the velocity measurements were made approximately 25.4 mm from the front side-wall. Flowfield measurements were first made across the depth of the test section to ensure that the measurements reported were not influenced by the side-wall boundary layer. Typical operating temperatures were maintained at 24 °C ± 1 °C.

A two-component LDV system was used to measure the mean velocities in the louvered fin array. The focal length of the lens is 350 mm, with a probe volume that is 90 μm in diameter and 1.3 mm in length. Incense smoke, generated outside the main loop and injected just upstream of the settling chamber, was used to seed the flow. Mean horizontal and vertical

velocity components were obtained by sampling 5,000 points taken over a 15-20-second period at each measurement location. The bias uncertainty in the velocity measurements was estimated at 1%, arising from uncertainties in the Doppler frequencies and the fringe spacing. The velocity precision error, with a 95% confidence interval, was a maximum of 0.1%. The estimated uncertainty in the measured flow angle, obtained from measured velocity components, was 1.7%.

Figure 2b shows three rows of louvers in the test section and the positions at which velocity profiles were measured (referred to as 'cuts'). Due to the beams becoming blocked by the upper or lower louver as they are approached, the resulting bulk flowfield data covered 75% of the vertical louver passage (H_1 in Figure 1c). The remaining 25% of the flowfield, including the boundary layer measurements, were taken by tilting the LDV optics at the same angle as the louver angle and measuring the velocity component parallel to the louver (H_2 in Figure 1c). For the bulkflow measurements in the inlet louver, cuts were taken at the center of the horizontal portion (cut 1a) and at the center of the angled portion (cut 1b) in the stream-wise direction. The cut for the second louver was at the center in the stream-wise direction (cut 2). Five cuts were taken in the fifth louver (cuts 5a-e) to document the flow as it passes through a passage where the flow is considered to be "fully-developed".

Boundary layer measurements were only taken on the fifth streamwise louver, where the flow is considered fully developed. These measurements were characterized at four different positions on the louver at the same two Reynolds numbers (Re_{Lp} = 230 and 1016) as those used for the bulk flow measurements. The four positions included both the leading and trailing edge on both the front (upstream) side of the louver and the back (downstream) side of the louver. The leading edge measurements were taken at a streamwise position along the louver of $S/L_p = 0.14$ while the trailing edge measurements were taken at a streamwise position along the louver of $S/L_p = 0.86$. These are designated in Figure 1c as front leading edge (FLE), front trailing edge (FTE), back leading edge (BLE) and back trailing edge (BTE).

The CFD computations were performed using FLUENT/UNS, which adopts a pressure-based finite volume scheme. The flow for all of the computations presented in this paper was considered to be two-dimensional, steady or unsteady and laminar. The computational domain considered was limited to one complete row (17 louvers) with periodic boundary conditions on the top and bottom boundaries. The inlet boundary, with both a uniform velocity and a uniform temperature, was set at $1.5L_P$ upstream of the first louver. The outlet boundary, with negligible variation for both velocity and temperature in the streamwise direction, was set at $7L_P$ downstream of the last louver.

Conditions of no slip and no penetration as well as an isothermal boundary were applied to the louvered fin surfaces. The grid was generated using the code's unstructured triangular mesh generator. The discretized equations were solved using the SIMPLE algorithm with second order accuracy. Grid independence was achieved through both grid adaptation and grid resolution studies, (see Springer *et al.*, 1998). Typical grid sizes used in the current study varied from approximately 290,000 to 400,000 cells, depending on the simulated Reynolds number used.

RESULTS AND DISCUSSION

Bulk Flow Characteristics

This section briefly discusses the comparison of bulk flow characteristics between those measured by LDV and computed by CFD. As mentioned in the previous section, horizontal and vertical velocity components were measured at various louver locations to determine the

development of bulk flow profiles. Due to space limitations, only results at cuts 1a and 5c are presented here. More details are given in Springer *et al.* (1998). In the figures that follow, the ordinate plots a dimensionless vertical distance (Y/H_l) between two louvers (see Figure 1c). Here Y=0 corresponds to the center point between the two louvers. Note that normalization was done using H_l, such that the dimensionless ratio Y/H_l traverses from one louver wall to the other.

Figures 3a and 3b pertain to the cut made at the entrance to the inlet louver (cut 1a). Figure 3a compares predicted and experimental velocity profiles for both $Re_{Lp} = 230$ and $Re_{Lp} = 1016$, normalized with respect to inlet velocity (U_{in}). Figure 3b compares predicted and experimental local flow angles for both $Re_{Lp} = 230$ and $Re_{Lp} = 1016$, normalized with respect to louver angle (θ). Note that the local flow angle (α) was calculated using $\alpha = \tan^{-1}(v/u)$, where u and v are the x and y components of the flow velocity, respectively. Mean flow angles are based on an integrated average of the local values measured over 75% of the passage: α/θ is called the mean flow efficiency by Webb and Trauger (1991). At cut 1a, the figures show that the flow is uniform and is directed essentially in the streamwise direction (mean flow efficiency $\alpha/\theta < 0.1$). At $Re_{Lp} = 230$, the core flow has been accelerated to $1.4U_{in}$, while at $Re_{Lp} = 1016$, it is only $1.2U_{in}$. This higher acceleration at the lower Reynolds number is due to the thicker boundary layers that form on the louvers. The CFD predictions are seen to be in good agreement with the measured velocity profiles and local flow angles, especially at the lower Reynolds number. At $Re_{Lp} = 1016$, slightly higher core velocities are predicted than measured; this difference can be attributed to both 3D geometrical effects and the presence of the top and bottom walls in the experimental test section.

The flow has changed significantly by the second louver (cut 2) showing not only wake effects of the upstream louver, but also that it is mostly 'louver directed', even for the lower Reynolds number (Springer *et al.*, 1988). The local flow-to-louver angle ratios for cut 2 also show that the flow is essentially louver directed, with a mean flow efficiency $\alpha/\theta \approx 0.98$ for $Re_{Lp} = 230$ and 1.0 for $Re_{Lp} = 1016$ (see Springer et al., 1998).

By the fifth louver passage (cuts 5a-e), the flow has reached a fully-developed condition for both Reynolds numbers. Figures 4a and 4b compare predicted and experimental normalized velocity profiles and local flow-to-louver angle ratios for both Reynolds numbers at cut 5c. For $Re_{Lp} = 230$, there is not much change in the shape of the profile between the second and fifth louvers: a velocity deficit shows up at $Y/H_l \approx 0.1$ due to the immediate upstream louver. For $Re_{Lp} = 1016$, however, there is substantial change between the second and fifth louvers, with an *additional* velocity deficit at $Y/H_l \approx -0.2$, apparently due to the wake of the third louver (two louvers upstream). This deficit is weaker than that due to the louver immediately upstream, as expected. The CFD measurements capture these deficits nicely, although predictions are slightly higher than measurements for the same reasons as given above. Mean flow efficiencies are approximately 1, similar to the second louver. However, there is a discernible decrease in the local flow angle in the region of the stronger velocity deficit, especially for $Re_{Lp} = 230$, indicating the strong effects of the wake. Again, these local characteristics are well picked up by the CFD predictions.

Figure 5 shows CFD and LDV comparisons of mean flow efficiency for the louver array at $Re_{Lp} = 1016$. It can be seen that the mean flow efficiency has reached a value of approximately 1 by the second louver for both. This indicates that the flow has become louver directed earlier in the louver array than measured by Antoniou et al. (1990). However, this is expected since the F_P/L_P ratio of Antoniou et al. (1990) is more than double that presently used

(lower fin density). Even at the turning louver, the flow readjusts to louver directed flow by the louver immediately downstream. Although not shown here for clarity, similar results were also seen for Re_{Lp} = 230. More details on bulk flow characteristics and the comparisons made between LDV and CFD can be found in Springer et al. (1998).

Boundary Layer Characteristics

As mentioned above, the velocity component parallel to the louver (u_L) was measured by turning the LDV optics orthogonal to the louver. This velocity component was measured to characterize the boundary layer at four different locations around the fifth louver (FLE, FTE, BLE, BTE) at two different Reynolds numbers, Re_{Lp} = 230 and 1016. In the figures that follow, the ordinate plots a dimensionless normal distance (Y/H_2) from the upper and lower surface of the fifth louver (see Figure 1c). Here Y=0 corresponds to the surface of the louver. Note that normalization was done using H_2, such that the dimensionless ratio Y/H_2 varies from zero (at the louver wall) to ± 0.6 (60% across the passage, well into the bulk flow).

Figure 6a shows the measured and predicted velocity profiles in the boundary layer at Re_{Lp} = 230 for the leading and trailing edges for the front side of the louver. As before, the local velocity is normalized with the inlet velocity to the test section. As expected, as one passes along the fin, the boundary layer thickness increases, but even at the trailing edge, the extent of the boundary layer never exceeds half the normal distance between the louvers (this is true of all the boundary-layer measurements). It can also be seen that upstream louvers have no effect at Re_{Lp} = 230. The CFD predictions pick up the trends within the boundary layer very well, especially at the leading edge. As one moves into the bulk, the predicted results consistently indicate higher velocities than those measured (14% higher peak velocity), as reported above. Figure 6b shows the same information for the back of the louver. Here, the wake from the upstream louver is still evident at the leading edge at around Y/H_2 = -0.4 (bulk flow), making it difficult to define a boundary layer thickness. However, this deficit has all but disappeared by the trailing edge. If one compares figures 6a and 6b, the boundary layers are thicker on the back side of the louver as expected. Once again, CFD predicts the trends well, overpredicting a little at the trailing edge.

Figures 7a and 7b show the same boundary layer comparisons at a Reynolds number of 1016. For the front side in the bulk flow, the wake from two louvers upstream is now evident, as reported in the bulk flow measurements. For the back side, the wake from the immediate upstream louver is also clearly evident. CFD again predicts the trends in the boundary layer well, although the maximum velocity at the boundary layer edge is consistently significantly overpredicted. As before, this is thought to be as a result of the test section flow not being truly periodic in nature due to the presence of the upper and lower walls. Also picked up by CFD and not by experiment is a small recirculation zone on the BLE as seen in Figure 7b.

For both Reynolds numbers, significant differences occur in the boundary layer characteristics when comparing the front and back sides of the louver. This is consistent with past studies that have predicted differing local heat transfer coefficients on the front and back sides of the louver. For both Reynolds numbers, steeper velocity gradients (dU_L/dY) occur on the front side as compared with the back side. By invoking Reynolds' analogy, these steeper gradients would imply higher convective heat transfer on the front side of the louver.

Comparing the two different Reynolds numbers (Figures 6 and 7), thicker boundary layers develop along the louver for the Re_{Lp} = 230 case, as expected. Another important difference in the bulk flow is that the appearance of the wake for Re_{Lp} = 230 on the back side of

the louver only occurs at the leading edge, while the wake is evident at both the leading and trailing edges for $Re_{Lp} = 1016$. The trailing edge profiles at $Re_{Lp} = 230$, however, do not indicate a fully developed, laminar, parabolic flow.

Table 2 shows a comparison between measured and predicted boundary layer thicknesses. The edge of the boundary layer was taken to be the point of maximum velocity near the wall. The boundary layer thickness was then taken as the location where the velocity was 99% of the edge velocity. Except for the front leading edge (FLE) at the lower Reynolds number, the CFD predicted thicknesses are within ± 8% of the measured values. In addition to CFD predictions, the Blasius laminar, flat plate boundary layer solution was also calculated for comparison along the length of the louver. Differences here are much greater, especially at the trailing edge where Blasius greatly overpredicts. However, this can be explained since Blasius is for a single flat plate, where the boundary layer is not 'squeezed' by an upper plate as with the present case.

Table 2: Comparison of Blasius, CFD and measured boundary layer thicknesses

$Re_{Lp} = 230$	FLE	FTE	BLE	BTE
Measured $\delta_{99\%}$ Y/H_2	0.119	0.279	0.159	0.260
Blasius $\delta_{99\%}$ Y/H_2	0.172	0.390	0.170	0.424
CFD $\delta_{99\%}$ Y/H_2	0.149	0.260	0.161	0.255
$Re_{Lp} = 1016$	**FLE**	**FTE**	**BLE**	**BTE**
Measured $\delta_{99\%}$ Y/H_2	0.103	0.162	0.115	0.179
Blasius $\delta_{99\%}$ Y/H_2	0.088	0.206	0.089	0.211
CFD $\delta_{99\%}$ Y/H_2	0.103	0.154	0.125	0.171

Impact on Heat Transfer

Based on the good agreement between the CFD and LDV results, and to promote discussion as to the impact that these results have on actual heat exchanger performance, CFD calculations have been performed over a wider range of Reynolds numbers ($50 < Re_{Lp} < 2000$). These values correspond to inlet face velocities between 0.7 m/s and 26.6 m/s (≈ 1.5 to 59 mph). Figure 8 shows these predicted Colburn j factors, together with analytical solutions for both flow over a flat plate (based on Blasius with a plate length of L_p) and fully developed laminar duct flow (with a duct height of F_p). For the two Reynolds numbers used in the current experimental investigation, the combined CFD and LDV analysis clearly confirms that both flows are in the steady laminar region and that both are dominated by louver directed flow.

Figure 8 shows the similarity in slope between the CFD predicted data and that for flow over a flat plate. As identified by the LDV measurements above, this region has been shown to be "louver directed". The similarity in slope would seem to indicate that the flow characteristics of louver directed flow are therefore more similar to that for flow over a flat plate than fully developed duct flow. This is consistent with that previously reported by Achaichia and Cowell

(1988a), who indicated that for $Re_{Lp} > 200$, their experimental measurements showed characteristics similar to that of flow over a flat plate.

At lower Reynolds numbers ($50 < Re_{Lp} < 200$), Achaichia and Cowell (1988a) showed that the flow regime goes through a transition region from "duct directed" to "louver directed" flows. Although no clear-cut "duct directed" flow was observed for the Reynolds numbers simulated here, the curve does indicate the start of a transition region for $Re_{Lp} < 100$. At the highest Reynolds number of 2000, the flow is found to be unsteady with vortex shedding from the last louver in the array. This vortex shedding moves upstream as Reynolds number is further increased, consistent with the numerical study of Tafti *et al.* (1998): however, this remains to be validated experimentally.

Also shown in Figure 8 is some test data from an actual automotive PF style heat exchanger with fin geometry equal to that given in Table 1 (Hughes, 1998). Although, the two-dimensional CFD predicted data differ quantitatively from those of the actual three-dimensional heat exchanger, the trends are very similar. The differences are attributed to the presence of the tubes in the actual heat exchanger. Boundary layers grow from these tube surfaces in addition to those developing along the fin surfaces. At lower Reynolds numbers, the boundary layers on the tube surfaces are relatively thick and the effect of three-dimensionality will be more evident. As a result of this, the difference between the test data and CFD predictions will tend to be more significant at low Reynolds numbers, diminishing as Reynolds number increases as seen in Figure 8. Note that the exceptionally good agreement between the actual test data and the analytical solution over a two-dimensional flat plate is considered to be coincidental. However, both are lower than the 2-D CFD data, indicative of thicker boundary layers. For the Blasius flat plate solution, evidence of thicker boundary layers is presented above in Table 2.

CONCLUSIONS

Detailed experimental bulk flowfield and boundary layer measurements in a 20:1 scaled-up model of a complex louvered fin array have been successfully taken using LDV techniques. These measurements have been used as benchmarks for CFD computations, with good agreement found for both bulk flow and boundary layer velocity profiles. For the two Reynolds numbers studied ($Re_{Lp} = 230$ and 1016), the flow was found to be "louver directed" and became fully-developed by the fifth louver of a seventeen louver array.

For both Reynolds numbers, effects of the wake from the immediate upstream louver were evident. At $Re_{Lp} = 1016$, the flow entering the passage was also affected by the wake from two louvers upstream. The CFD predictions accurately capture these velocity deficits. Over-prediction of maximum velocities was evident in the bulk flow and thought to be due to the difference between the actual test section geometry and the periodic boundary conditions chosen for the CFD study. Additional CFD heat transfer predictions verify that the dominating heat transfer enhancement mechanisms in this Reynolds number range are the continuous restart of the boundary layer and the directing of flow along the louvers.

NOMENCLATURE

F_P = fin pitch
H_1 = vertical distance between louvers, $F_P - (t/\cos\theta)$
H_2 = normal distance between louvers, $H_1 \cos\theta$
j = Colburn j factor
L_P = louver pitch

t = fin thickness
u = streamwise velocity component
U = total velocity magnitude
U_{in} = inlet velocity to test section
u_L = velocity component parallel to louver
v = vertical velocity component
Y = vertical coordinate direction relative to louver
α = flow angle
θ = louver angle

REFERENCES

Achaichia, A. and Cowell, T. A. (1988a) Heat Transfer and Pressure Drop Characteristics of Flat Tube and Louvered Plate Fin Surfaces, *Experimental Thermal Fluid Science*, vol. 1, pp. 147-157.

Achaichia, A. and Cowell, T. A. (1988b) A Finite Difference Analysis of Fully Developed Periodic Laminar Flow in Inclined Louvered Arrays, *Proceedings of 2nd UK National Heat Transfer Conference,* Glasgow, Vol. 2, ppl. 883-888.

Antoniou, A. A., Heikal, M. R., and Cowell T. A. (1990) Measurements of Local Velocity and Turbulence Levels in Arrays of Louvered Plate Fins, *Heat Transfer*, Paper No. 10-EH-18, pp. 105-110.

Beauvais, F. N. (1965) An Aerodynamic Look at Automobile Radiators, SAE Paper No. 650470.

Davenport, C. J.(1983) Correlations for Heat Transfer and Flow Friction Characteristics of Louvered Fins, Heat Transfer-Seattle, AICHE Symp. Series, No. 225, vol. 79, pp. 19-27.

Hughes, G. G. (1998) Private Communication (unpublished data), Modine Manufacturing Company, Racine, Wisconsin.

Springer, M. E. and Thole, K. A. (1998) Experimental Design for Flowfield Studies of Louved Fins, (in press) *Experimental Thermal and Fluid Science.*

Springer, M. E., Thole, K. A., Zhang, L. W., Memory, S. B. and Wattelet, J. P. (1998) A Combined Experimental and Computational Study of Flowfields in Louvered Fin Heat Exchangers, *Proceedings of 1998 ASME Fluids Engineering Division Summer Meeting,* Paper Number FEDSM98-4843, June 21-25, 1998, Washington, D. C.

Suga, K. and Aoki, H. (1991) Numerical Study on Heat Transfer and Pressure Drop in Multilouvered Fins, *ASME/JSME Thermal Engineering Proceedings*, Vol. 4, pp. 361-368.

Tafti, D. K., Wang, G. and Lin, W. (1998) Transitional Flow and Heat Transfer Characteristics of Developing Flow in Louvered Fin Array, *Proceedings of Heat Exchangers for Sustainable Development,* pp. 339-348, June 15-18, 1998, Lisbon, Portugal.

Webb, R. L. and Trauger, P. (1991) Flow Structure in the Louvered Fin Heat Exchanger Geometry, *Experimental Thermal and Fluid Science,* Vol. 4, pp. 205-217.

Zhang, L. W. (1996) A Numerical Study of Flow and Heat Transfer in Compact Heat Exchanger, *Ph.D. Thesis,* University of Illinois at Urbana-Champaign, Urbana, Illinois.

LIST OF FIGURES

Figure 2b	Louver orientation and measurement cut locations
Figure 3a,b	Velocity magnitude and local flow-to-louver angle ratio for developing flow in the first louver at Re_{Lp} = 230 and 1016
Figure 4a,b	Velocity magnitude and local flow-to-louver angle ratio for fully-developed flow in the fifth louver at Re_{Lp} = 230 and Re_{Lp} = 1016
Figure 5	Measured and predicted mean flow efficiency for the louver array at Re_{Lp} = 1016
Figure 6a,b	Measured and predicted velocity profiles in the boundary layer on the front and back sides of the fifth louver at Re_{Lp} = 230
Figure 7a,b	Measured and predicted velocity profiles in the boundary layer on the front and back sides of the fifth louver at Re_{Lp} =1016
Figure 8	Comparison of heat transfer results

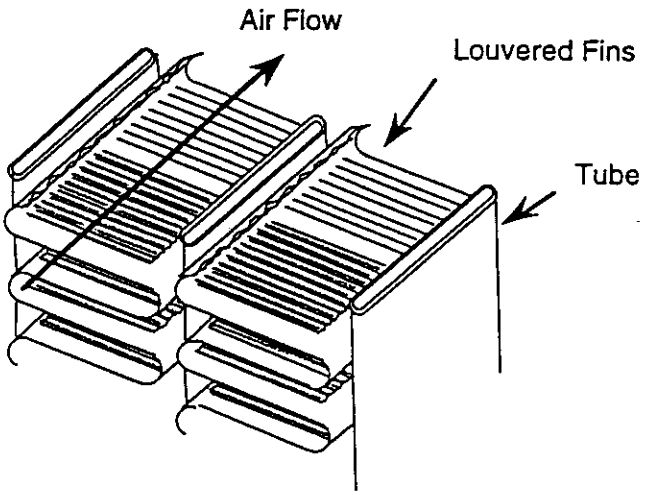
Air Flow
Louvered Fins
Tube

(a)

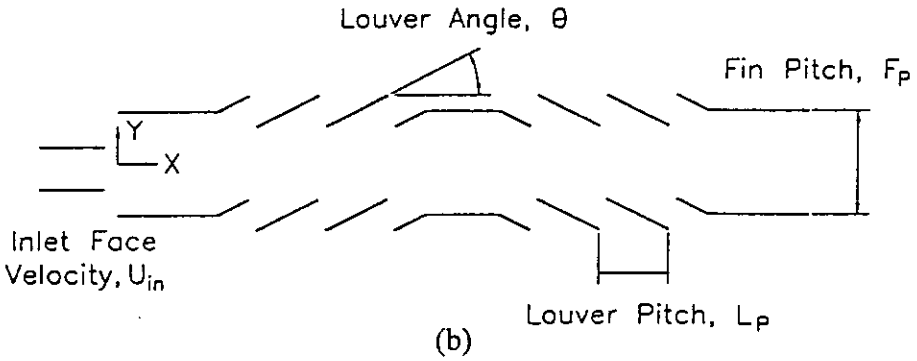
Louver Angle, θ
Fin Pitch, F_P
Y
X
Inlet Face
Velocity, U_{in}
Louver Pitch, L_P

(b)

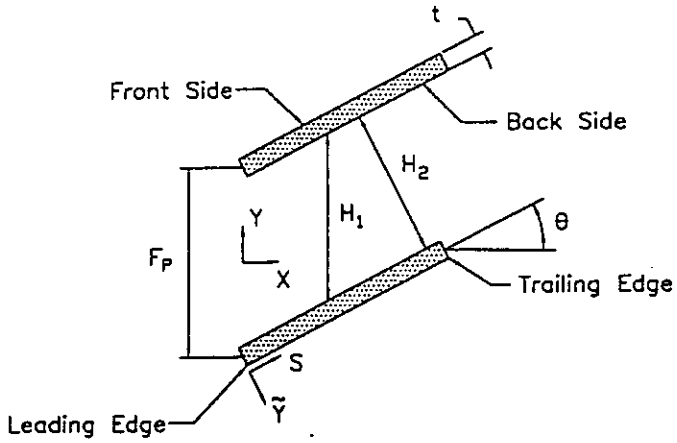
t
Front Side
Back Side
H_2
H_1
θ
Y
X
F_P
Trailing Edge
S
$\tilde{Y}$
Leading Edge

(c)

Fig. 1.

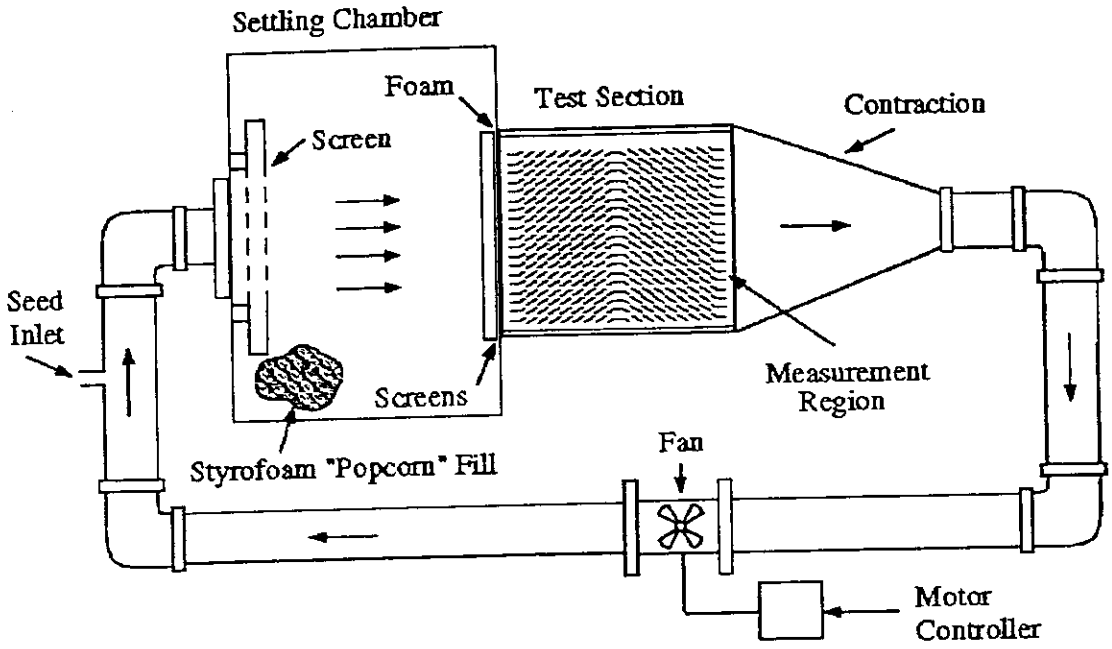
Settling Chamber
Foam
Test Section
Contraction
Screen
Seed
Inlet
Screens
Measurement
Region
Styrofoam "Popcorn" Fill
Fan
Motor
Controller

(a)

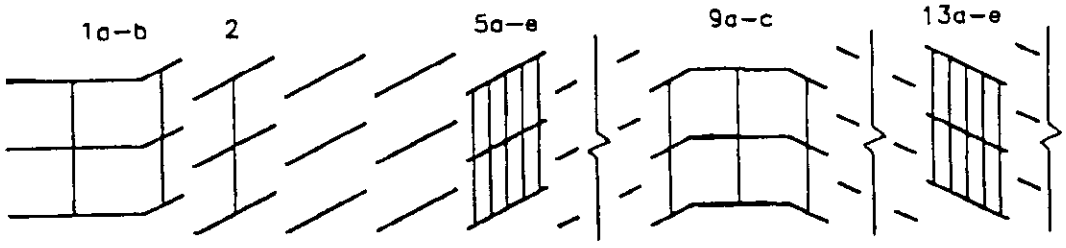
1a-b
2
5a-e
9a-c
13a-e

(b)

Fig. 2

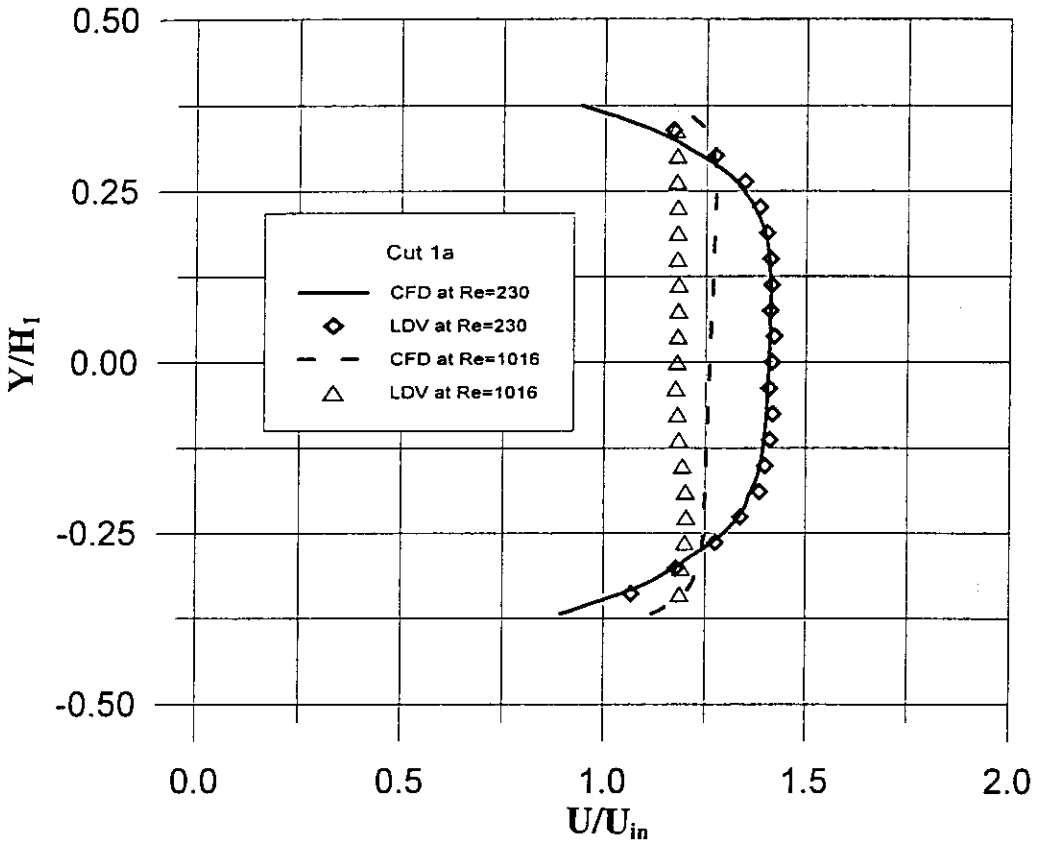
0.50
0.25
0.00
-0.25
-0.50
Y/H1
0.0
0.5
1.0
1.5
2.0
U/Uin
Cut 1a
CFD at Re=230
LDV at Re=230
CFD at Re=1016
LDV at Re=1016

Fig. 3a

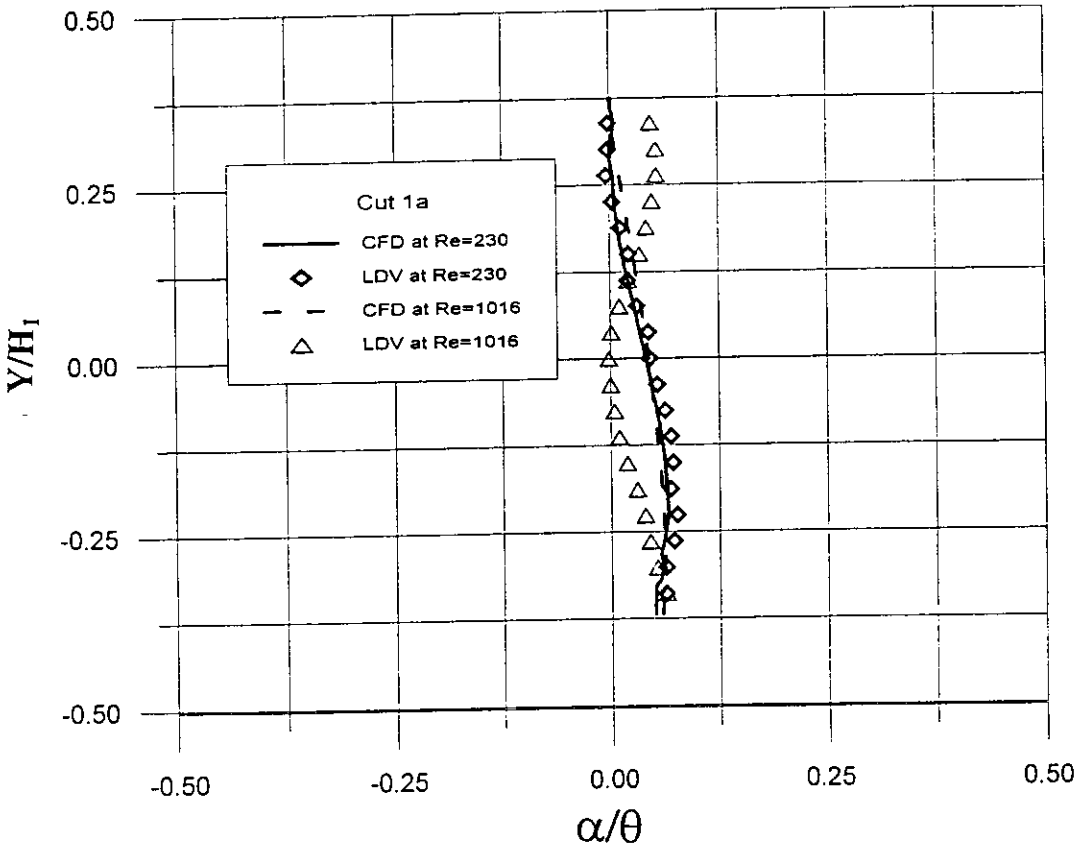
0.50
0.25
0.00
-0.25
-0.50
Y/H1
Cut 1a
CFD at Re=230
LDV at Re=230
CFD at Re=1016
LDV at Re=1016
-0.50
-0.25
0.00
0.25
0.50
α/θ

Fig. 3b

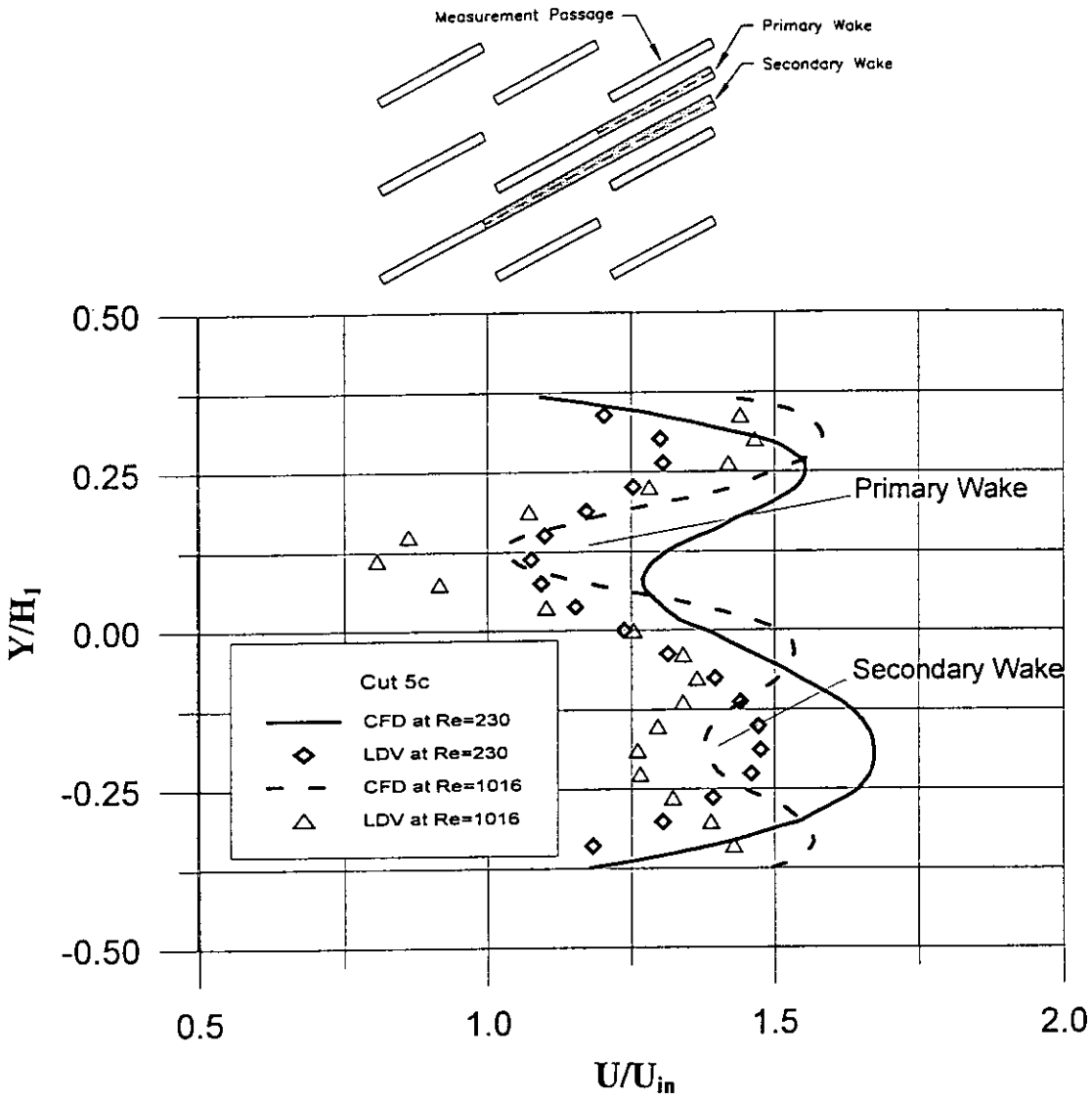
Measurement Passage
Primary Wake
Secondary Wake
0.50
0.25
0.00
-0.25
-0.50
Y/H1
0.5
1.0
1.5
2.0
U/Uin
Primary Wake
Secondary Wake
Cut 5c
CFD at Re=230
LDV at Re=230
CFD at Re=1016
LDV at Re=1016

Fig. 4a

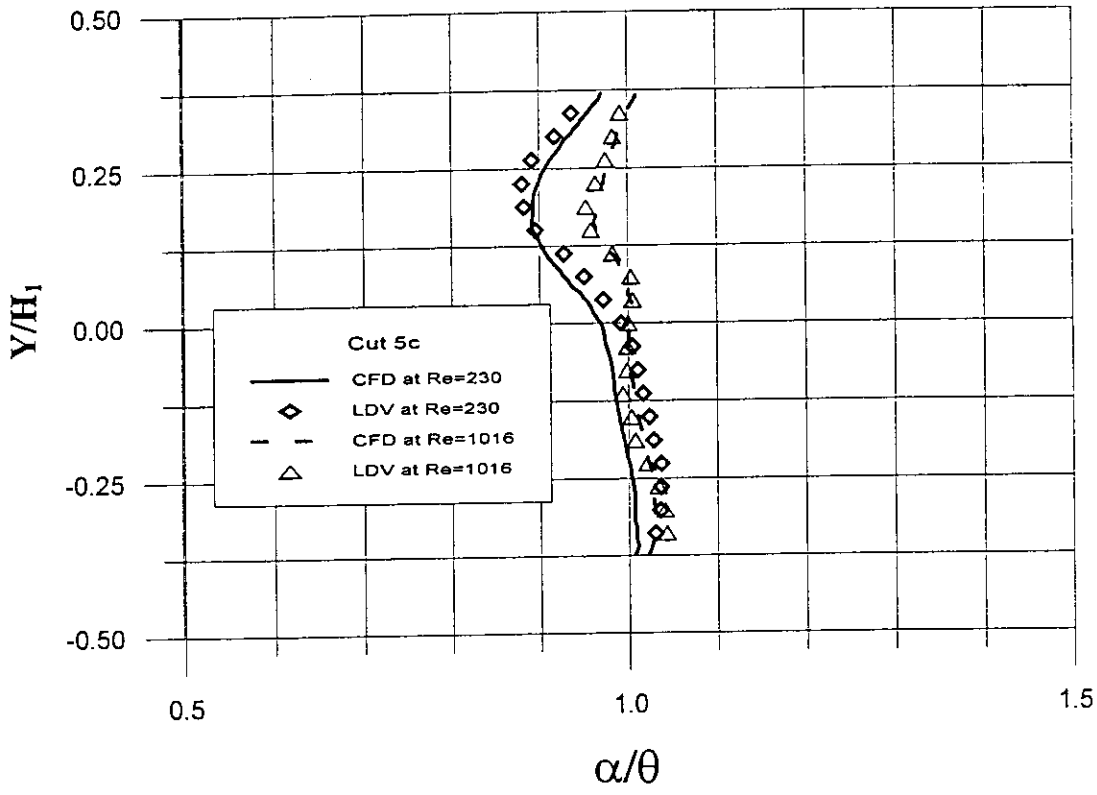
0.50
0.25
0.00
-0.25
-0.50
Y/H1
0.5
1.0
1.5
α/θ
Cut 5c
CFD at Re=230
LDV at Re=230
CFD at Re=1016
LDV at Re=1016

Fig. 4b

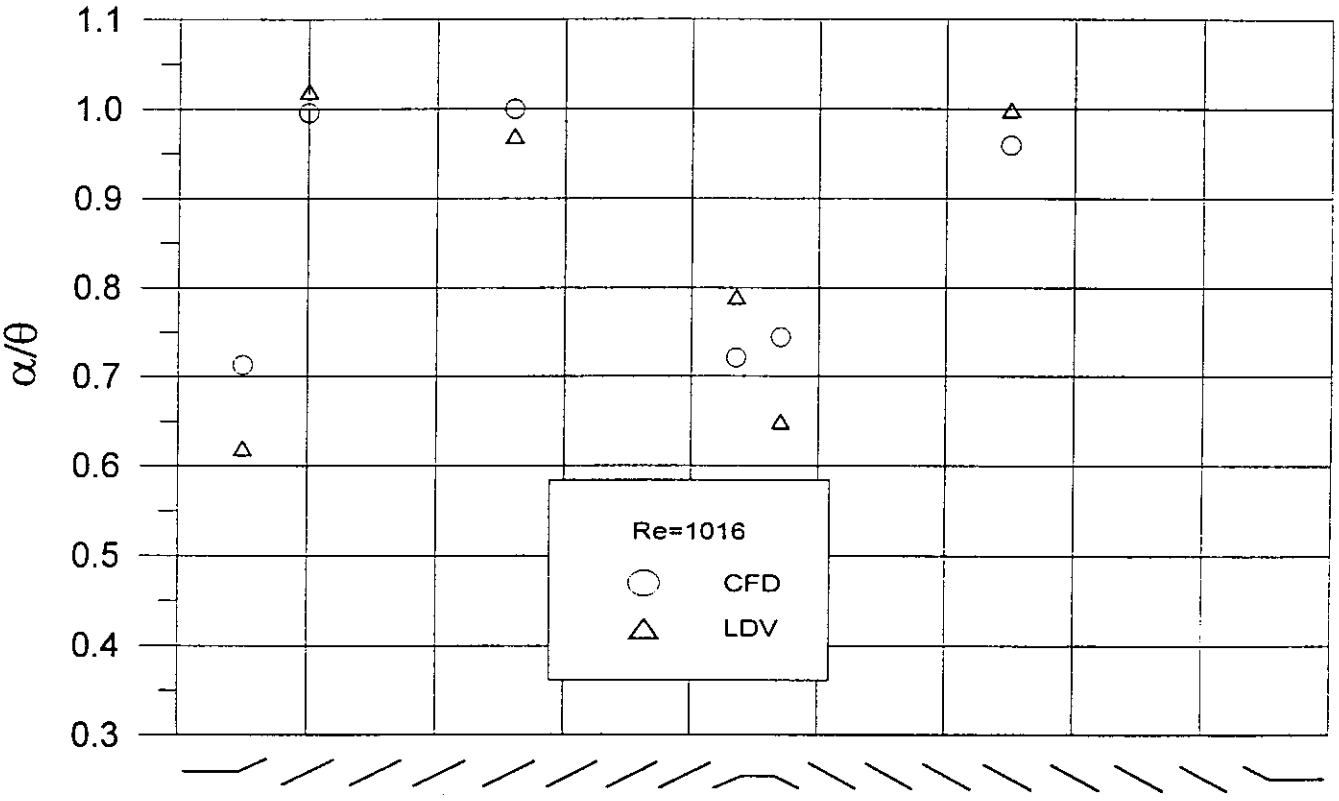

Fig 5

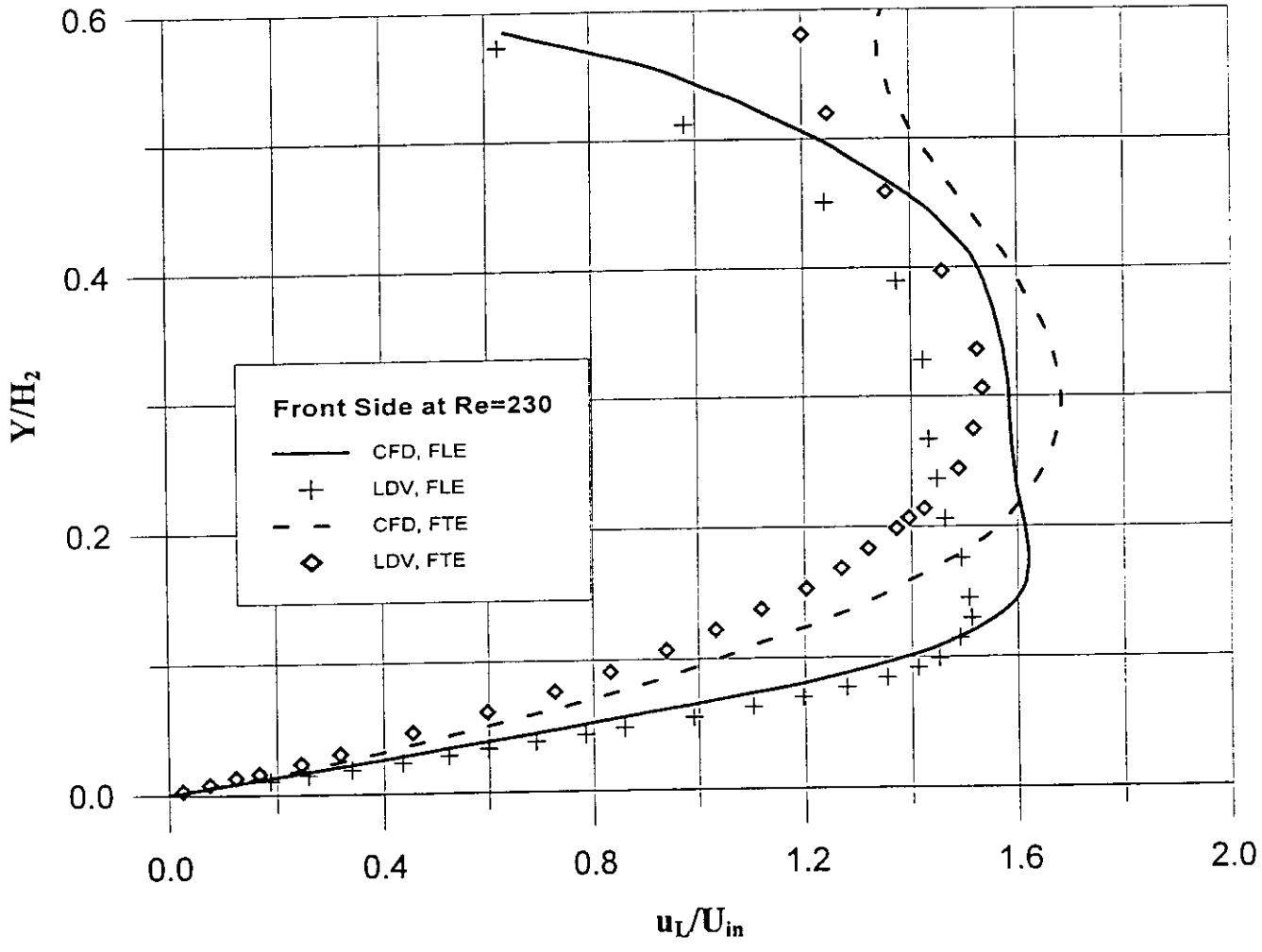
0.6
0.4
0.2
0.0
Y/H2
Front Side at Re=230
CFD, FLE
LDV, FLE
CFD, FTE
LDV, FTE
0.0
0.4
0.8
1.2
1.6
2.0
uL/Uin

Fig. 6a

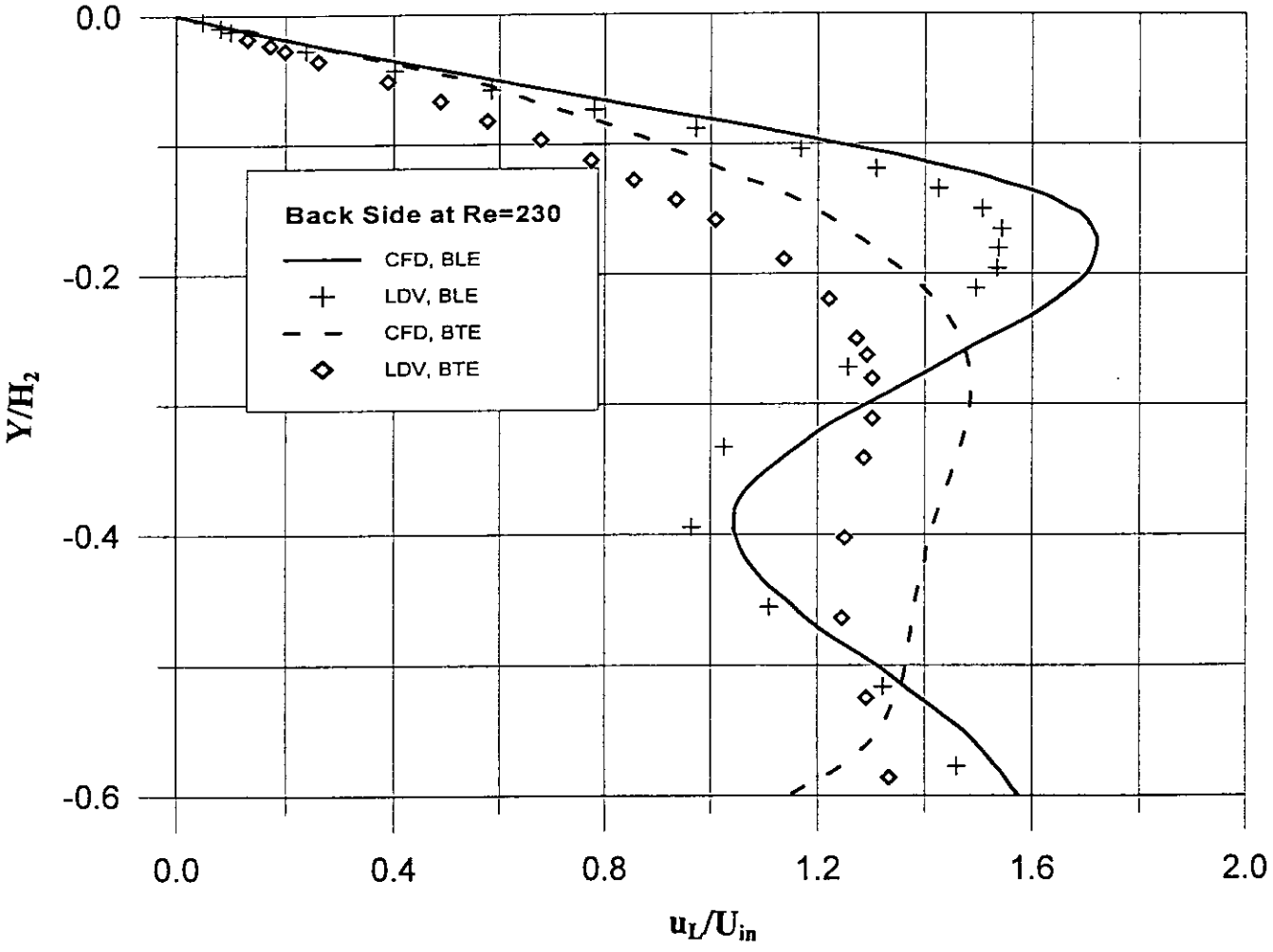
Back Side at Re=230
CFD, BLE
LDV, BLE
CFD, BTE
LDV, BTE
0.0
-0.2
-0.4
-0.6
Y/H2
0.0
0.4
0.8
1.2
1.6
2.0
uL/Uin

Fig. 6b

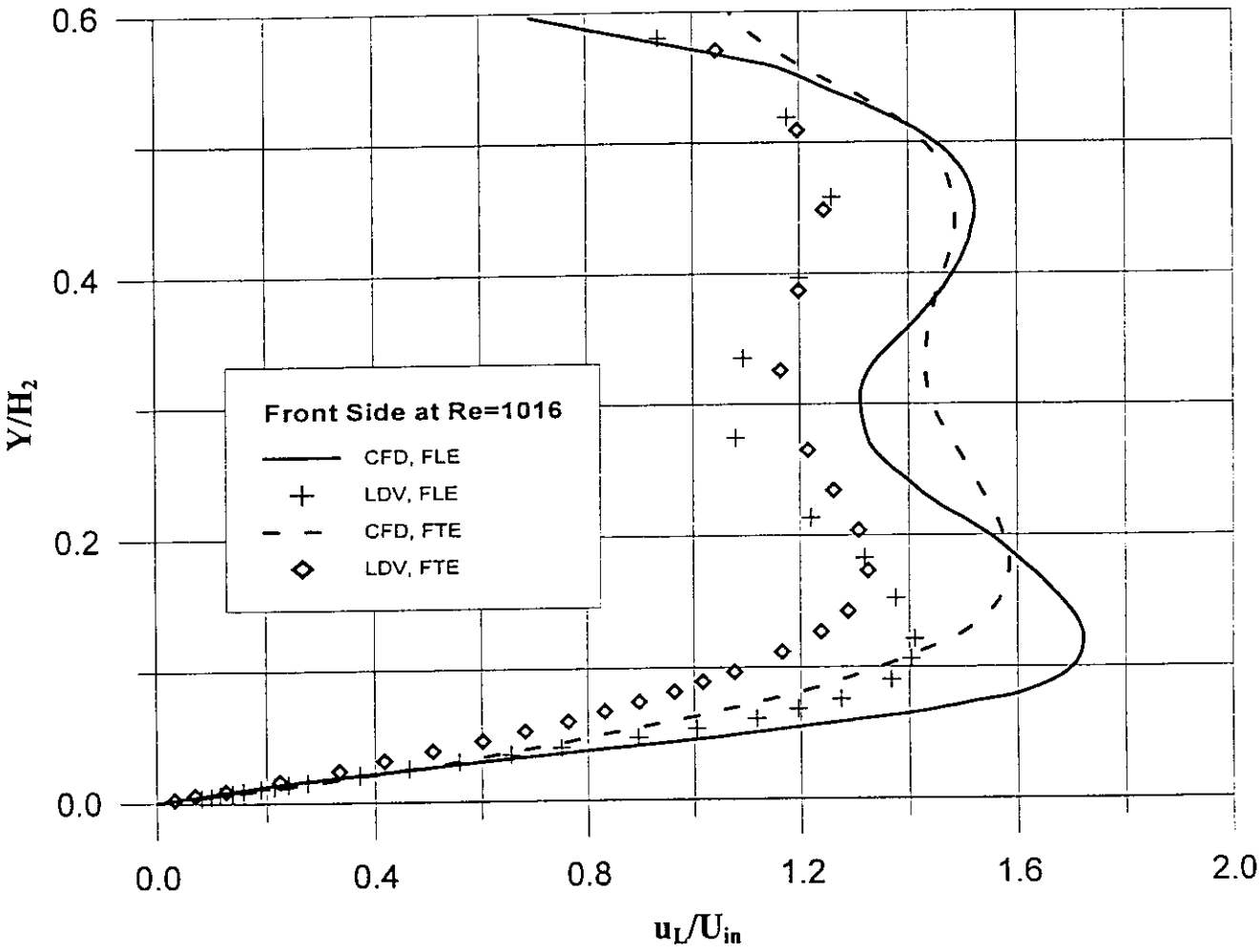
0.6
0.4
0.2
0.0
Y/H2
Front Side at Re=1016
CFD, FLE
LDV, FLE
CFD, FTE
LDV, FTE
0.0
0.4
0.8
1.2
1.6
2.0
uL/Uin

Fig. 7a

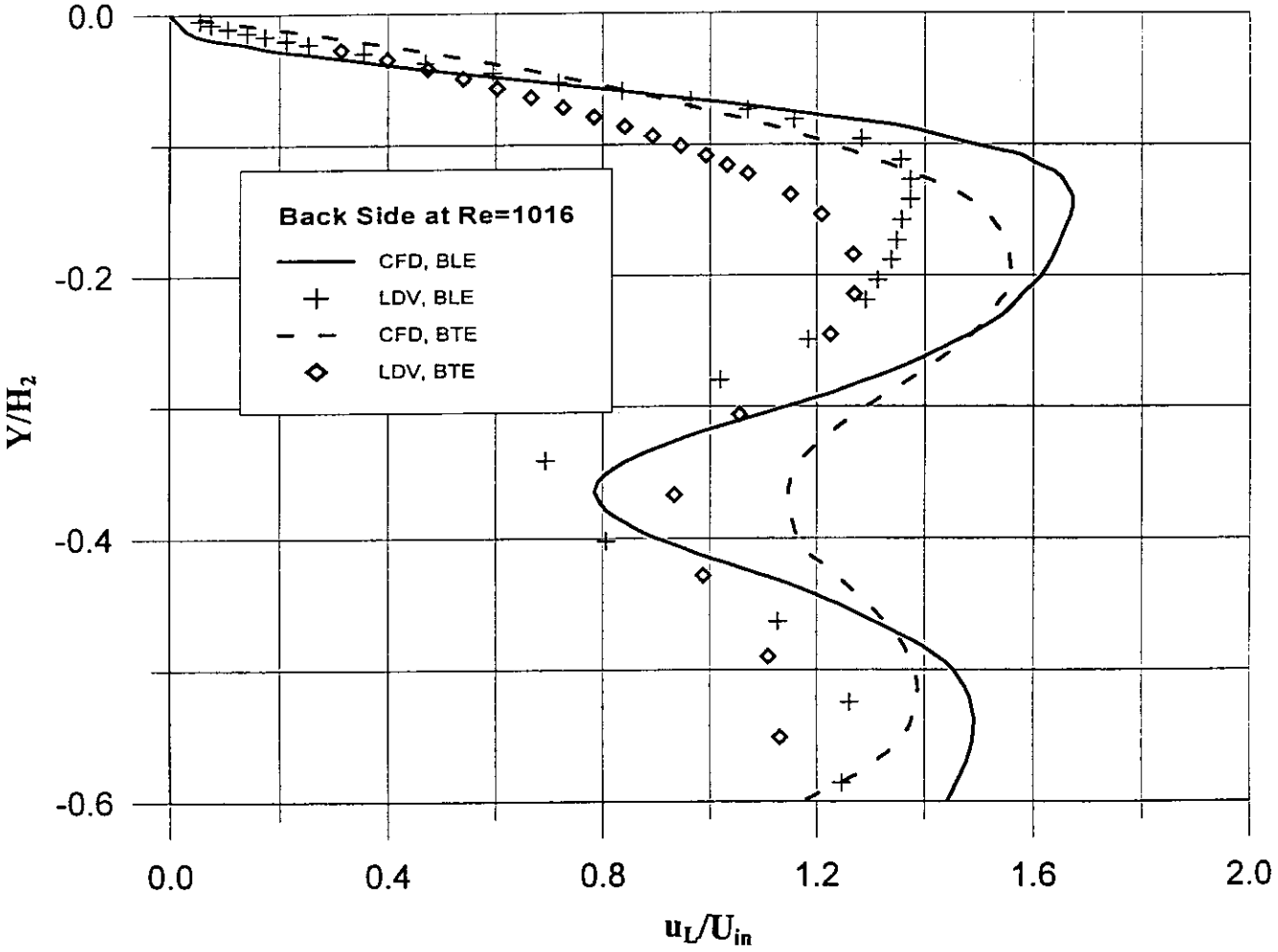
Back Side at Re=1016
CFD, BLE
LDV, BLE
CFD, BTE
LDV, BTE
0.0
-0.2
-0.4
-0.6
Y/H2
0.0
0.4
0.8
1.2
1.6
2.0
uL/Uin

Fig. 7b

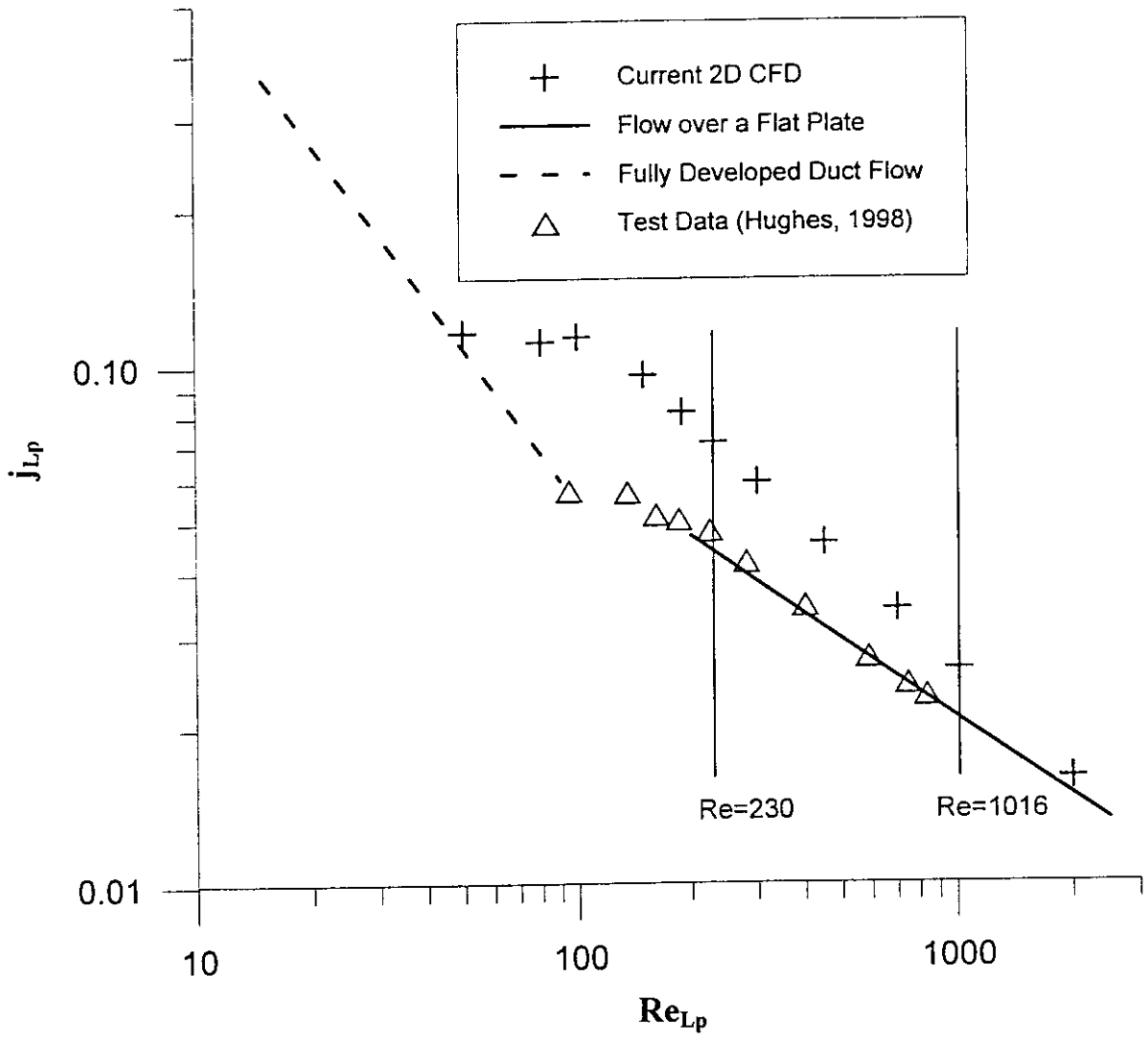
Current 2D CFD
Flow over a Flat Plate
Fully Developed Duct Flow
Test Data (Hughes, 1998)
0.10
0.01
j_{Lp}
Re=230
Re=1016
10
100
1000
Re_{Lp}

Fig. 8